Dalton Transactions

PAPER

View Article Online
View Journal | View Issue

Cite this: *Dalton Trans.*, 2014, **43**, 10628

Peculiar behavior of MWW materials in aldol condensation of furfural and acetone

Oleg Kikhtyanin,[a] Pavla Chlubná,[b] Tereza Jindrová[a] and David Kubička*[a]

Received 19th January 2014,
Accepted 23rd April 2014

DOI: 10.1039/c4dt00184b

www.rsc.org/dalton

MWW family of different structural types (MCM-22, MCM-49, MCM-56 and MCM-36) was used as catalysts for aldol condensation of furfural and acetone studied in a batch reactor at 100 °C, autogenous pressure and a reaction time of 0–4 h. To establish a relation between physico-chemical and catalytic properties of microporous materials, the samples were characterized by XRD, SEM, N_2 adsorption, FTIR and TGA. It was found that the acidic solids possessed appreciable activity in the reaction and resulted in the formation of products of aldehyde–ketone interaction. Surprisingly, MCM-22 and MCM-49, *i.e.* three-dimensional materials containing internal supercages, exhibited higher activity than two MCM-36 catalysts with two-dimensional character having larger accessible external surface area due to expansion of the interlayer space by swelling and pillaring treatments. Moreover, all MWW family catalysts gave higher conversion than the large-pore zeolite BEA. Nevertheless, furfural conversion decreased rapidly for all the studied materials due to coke formation. Unexpectedly, the deactivation was found to be more severe for MCM-36 catalysts than for MCM-22 and MCM-49, which was attributed to the reaction taking place also in supercages that are protected by 10-ring channels from severe coking. In contrast the cups located on the external surface were coked rapidly.

1. Introduction

Production of valuable chemicals as well as fuels from renewable raw materials is a key technological challenge facing modern society at the beginning of the 21st century. The development of efficient technologies, relying on the use of natural renewable resources, is an essential step for ensuring social security and stability and mitigating the increasing environmental threats connected with the extensive use of fossil fuels.[1]

Transformation of lignocellulosic and, in particular, waste biomass into fuels and valuable chemicals is considered to be one of the most promising directions as it allows avoiding competition with food and fodder production.[1,2] Cellulose-rich feedstocks can be successively treated to form different monomeric products, generally sugars.[3–5] These can be further converted by acid hydrolysis to furanic compounds (furfural or hydroxymethylfurfural) that can serve as platform chemicals in many applications.[6–8] Among them, aldol condensation has great potential as it allows increasing the carbon atom chain length beyond six carbon atoms, which is the limit for sugars. Furanic compounds thus can be valorized by aldol condensation with acetone in the presence of suitable heterogeneous catalysts like MgO–ZrO_2,[7] alkali and alkaline earth oxides,[9–15] alkali-exchanged zeolites (Cs-BEA),[16] MCM41,[17,18] aluminophosphate oxynitrides,[19] ion-exchange resins,[20,21] and activated Mg–Al hydrotalcites.[22–26] Alternatively, a biphasic system with NaOH as a catalyst was also proposed.[27] The needed acetone may be obtained by ketonization of acetic acid[28] that is an important product of biomass pyrolysis. This route has attracted significant interest, because hydrogenation/hydrodeoxygenation of these aldol condensation products leads to various hydrocarbons suitable for blending in conventional diesel fuel and kerosene.[29]

Aldol condensation of aldehydes and ketones is a classical reaction of organic synthesis, which takes place in the presence of both acidic and basic catalysts. Homogeneous basic catalysts such as sodium hydroxide are most often used for this purpose.[29–31] They possess high activity in conversion of reactants and high selectivity towards the desired reaction products. Unfortunately, their environmental friendliness is not satisfactory, particularly for large scale applications, due to the need for neutralization and separation of the homogeneous catalysts from the liquid products. Consequently, solid basic catalysts have attracted widespread interest as they could be helpful in overcoming the deficiencies of the currently used catalysts. The most studied basic solid catalysts include metal oxides or double mixed oxides, such as MgO,[32]

[a]*Research Institute of Inorganic Chemistry, RENTECH-UniCRE, Chempark Litvínov, Záluží – Litvínov, 436 70, Czech Republic. E-mail: david.kubicka@vuanch.cz; Tel: +420-476163735*
[b]*J. Heyrovský Institute of Physical Chemistry, Academy of Sciences of the Czech Republic, v.v.i., Dolejškova 3, 182 23 Prague, Czech Republic*

$MgO–Al_2O_3$,[33–35] $MgO–ZrO_2$ [29,36] and TiO_2.[37] Recently, also MOFs have been recognized as highly active catalysts in different condensation reactions.[38,39] Despite the intensive research efforts, the heterogeneous basic catalysts suffer from several major drawbacks such as high sensitivity to the ambient CO_2 and difficulties connected with re-using the hydrotalcite-based catalysts in successive catalytic runs,[40–42] which limits their widespread industrial use. Therefore, along with the optimization of the properties of the solid basic catalysts, attention is focused on alternative solid catalysts for aldol condensation. In this respect, solid acid catalysts have been recognized as promising candidates.

Among solid acid catalysts, zeolites are considered versatile and tunable acidic catalysts exhibiting good activity and selectivity in various reactions of organic synthesis ranging from petrochemical to fine chemical applications.[1,43–48] Zeolites were also investigated as catalysts for aldol condensation in the past.[49–51] In our recent work[52] it was shown that the acidic zeolites possess rather good activity in aldol condensation of furfural and acetone and their catalytic properties are determined by the structural type, as well as by their textural and acidic characteristics. The highest conversion of furfural was observed when using wide pore zeolites with a three-dimensional crystalline framework, the best result being obtained over zeolite BEA. It was also shown that during the reaction, the activity of all investigated zeolites decreased due to the formation of carbonaceous deposits inside their micropores. Therefore, to compete with the solid basic materials as catalysts for aldol condensation it is necessary to optimize the properties of zeolites with the aim to increase their activity in the reaction and to improve their stability, *i.e.* resistance to coking. Layered two-dimensional materials exhibit a better accessibility of their active sites than the classical three-dimensional zeolites and could thus make the activity enhancement possible. About fifteen zeolite frameworks have been found to form two-dimensional zeolite forms and among them MWW is the first and most famous example.[53–56]

In this respect, materials with MWW framework topology occupy a special place among a large variety of different micro- and mesoporous materials as this family consists of more than ten members, *e.g.* MCM-22, MCM-36, MCM-49, MCM-56 and others, which have the same MWW topology but a different arrangement of the layers (different interlayer bonding and distances).[57] The unifying feature of all MWW materials is the presence a layered crystalline unit in their structure, so-called "MWW monolayer", with a thickness of 25 Å, which contains a two-dimensional 10-MR sinusoidal channel pore system and large cups (7.1 Å Ø, 7.0 Å depth) on the [0 0 1] crystal surface.[58,59] As a result of agglomeration of such layered species during hydrothermal treatment of aluminosilicate gel in the presence of hexamethyleneimine (HMI) an intermediate product is formed. It is designated as MCM-22 (P), the layered precursor. Upon calcination of this reaction product, the condensation of the monolayers occurs leading to creation of a new independent pore system, constituted by large supercages (7.1 Å Ø, 18.2 Å height) accessible through 10-ring openings (4.0 Å × 5.5 Å),[58] thus forming a three-dimensional crystal framework of MCM-22 zeolite with two independent pore systems.

Formation of MCM-36 occurs through the subsequent swelling of the MCM-22(P) precursor by the addition of cetyltrimethylammonium hydroxide followed by pillaring treatment using tetraethoxysilane (TEOS).[53,60] As a consequence, the space between the "MWW monolayers" is expanded and internal mesoporous space is generated. Thus, MCM-36 provides free access to all large cups, located on the external surface of "MWW monolayers". Nevertheless, it should be underlined that the pillars consist of amorphous and inactive silica and thus they dilute the concentration of active sites. Their nature remains unknown.

Zeolite MCM-49 possesses nearly the same framework topology as the calcined MCM-22 (only the average unit cell *c*-parameter is 0.2 Å longer in MCM-49).[61] However, unlike the latter, MCM-49 is formed by a direct synthesis route, avoiding the formation of intermediate lamellar MCM-22(P). This is achieved by optimizing the composition of the initial reaction mixture and the conditions of its hydrothermal treatment. When hexamethyleneimine is used as a structure directing agent, MCM-49 generally has a lower Si/Al molar ratio (<13) than MCM-22P does (>13). A factor that influences the formation of either MCM-22P or MCM-49 is the molar ratio of the organic cation R_o (SDA) to the inorganic cations R_i (*e.g.* Na, K, or Rb). When the ratio R_o/R_i is typically less than 2.0, the formation of MCM-49 is favoured. By analogy with MCM-22, the crystalline framework of MCM-49 consists of two independent pore systems, which are both accessible through 10-ring apertures with diameters of 4.0 × 5.9 Å for the sinusoidal channels and 4.0 × 5.4 Å for the entrances to the supercages.[62]

Apart from MCM-22, zeolite MCM-49 crystallizes through its delaminated intermediate designated as MCM-56. MCM-56 is synthesized from the same synthetic gel as MCM-49 but with a more careful control for crystallization time and temperature.[63] The structure of this zeolite consists of disordered agglomeration of "MWW monolayers" without in-registry alignment in the *c* direction and no interlayer links. Due to this, MCM-56 has a higher concentration of large cups exposed to the crystal surface than the MCM-49.

Owing to their properties, MWW materials have been used in a number of different applications, and it has been found that they can be considered promising catalysts for several organic reactions, for example for isobutene–2-butene alkylation,[64] as well as alkylation of benzene with propylene.[65] The uniqueness of these catalysts is that they combine the properties of both conventional zeolite systems and layered materials. The expansion of the areas of application of MWW materials necessitates a deeper understanding of the impact of structural features on their activity in conversion of organic molecules.

This paper presents a comparative study focusing on (i) characterization of MCM-22, MCM-36, MCM-49 and MCM-56 materials with a number of physico-chemical methods, and (ii) investigation of their catalytic properties in aldol condensation

of furfural and acetone. In addition, wide-pore zeolite Beta that has shown the best performance among the zeolite catalysts investigated previously in aldol condensation of furfural and acetone was included in the study for comparison.

2. Experimental

2.1. Synthesis of MWW materials

2.1.1. MCM-22. 7.31 g of 50% water solution of NaOH was added to 400 g of water. 7.44 g of sodium aluminate (40–45% Na_2O, 50–56% Al_2O_3, Aldrich) was added and stirred until it dissolved. Then, 232.29 g of Ludox AS-30 was added. The mixture became thick and was stirred until a homogeneous gel was formed. Then, 38.34 g of HMI was added and the final mixture was stirred for 2 hours. The reaction mixture was charged into a Teflon-lined steel autoclave. Crystallization proceeded at 143 °C with inside stirring and autogenous pressure for 96 hours. The solid product was collected by filtration, washed with distilled water and dried in an oven at 60 °C overnight.

MCM-22P was heated in nitrogen at 500 °C for 3 hours and a temperature ramp of 2 °C min^{-1}, cooled to about 130 °C, and then calcined in air at 540 °C for 6 hours with the ramp of 2 °C min^{-1}. The calcined MCM-22 product was ion-exchanged into NH_4^+ form by treating four times with 1.0 M NH_4NO_3 solution for 4 hours at room temperature.

2.1.2. MCM-36(1). 1.16 g of NaOH was dissolved in 251.2 g of water and mixed with 1.68 g of sodium aluminate (40–45% Na_2O, 50–56% Al_2O_3, Aldrich). Then, 80 g of Ludox AS-30 was added. The mixture became thick and was stirred until a homogeneous gel was formed. Then, 38.34 g of HMI was added and the final mixture was stirred for 2 hours. The reaction mixture was charged into a Teflon-lined steel autoclave. Crystallization proceeded at 150 °C under agitation and autogenous pressure for 7 days. The solid product was collected by filtration, washed with distilled water and dried in the oven at 60 °C overnight.

10 g of uncalcined MCM-22(P) was added to 200 ml of 25% solution of C_{16}TMA-OH prepared by ion-exchange from chloride form. The slurry was stirred overnight at ambient temperature. The product MCM-22SW was separated by centrifugation, properly washed with water and dried at 60 °C.

Pillaring was carried out with 12.44 g of MCM-22SW in 373 ml of TEOS (Aldrich). The mixture was stirred and heated at 85 °C under reflux overnight. The solid was isolated by centrifugation and dried at ambient temperature. Then, about 1500 ml of water was added to 14.37 g of dried powder and stirred overnight (hydrolysis). The product was centrifuged again and dried at 60 °C. Final calcinations were carried out under nitrogen at 482 °C for 3 hours and a temperature ramp of 3 °C min^{-1}, cooled to about 130 °C and then calcined in air at 540 °C for 6 hours with a ramp of 2 °C min^{-1}. The calcined product MCM-36(1) was ion-exchanged into NH_4^+ form by treating four times with 1.0 M NH_4NO_3 solution for 4 hours at room temperature.

Table 1 Molar chemical compositions of reaction mixtures for the synthesis of MWW zeolites

Sample	Al_2O_3	SiO_2	Na_2O	HMI	H_2O
MCM-22	1	30	2.52	10	815
MCM-36(1)	1	46	3	20	1960
MCM-36(2)	1	36	3	20	1875
MCM-49	1	25	2.45	8.15	440
MCM-56	1	25	2.45	8.15	440

2.1.3. MCM-36(2). The preparation method of this sample was substantially the same as that for MCM-36(1), with the only exception that only 62 g of Ludox AS-30 was taken.

2.1.4. MCM-49. 9 g of 50% NaOH water solution was added to 396 g of water. 9.75 g of sodium aluminate (40–45% Na_2O, 50–56% Al_2O_3, Aldrich) was added and stirred until dissolving. Then, 77.1 g of silicon dioxide (Aldrich, nanopowder, particle size 10–20 nm) was added. The mixture was stirred for 10 minutes and then 40.8 g of HMI was added and the gel was stirred for 15 minutes. Crystallization proceeded at 143 °C under agitation and autogenous pressure for 93 hours. The solid product was collected by filtration, washed with distilled water and dried in the oven at 60 °C overnight.

MCM-49 was heated in nitrogen at 482 °C for 3 hours and a temperature ramp of 3 °C min^{-1}, cooled to about 130 °C, and then calcined in air at 540 °C for 6 hours with a ramp of 2 °C min^{-1}. The calcined product MCM-49 was ion-exchanged into NH_4^+ form by treating it four times with 1.0 M NH_4NO_3 solution for 4 hours at room temperature.

2.1.5. MCM-56. The preparation method of this sample was substantially the same as that for MCM-49, with the only exception that the time of hydrothermal synthesis was 33 hours.

Molar compositions of reaction mixtures used for the synthesis of different MWW samples are presented in Table 1. The relationship between different structures of the MWW family is depicted in Scheme 1.

2.2. Characterization methods

The crystallographic structures of MWW zeolites were determined by X-ray powder diffraction using a Bruker AXS D8 Advance diffractometer, working with the Cu K_α line (λ = 0.154 nm) in the 2θ range of 4–40°.

Nitrogen adsorption/desorption isotherms were measured on a Micromeritics GEMINI II 2370 volumetric Surface Area Analyzer at −196 °C to determine the surface area, pore volume and pore size distribution. Before the sorption measurements, all samples were degassed on a Micromeritics FlowPrep 060 instrument under helium at 300 °C (heating rate 10 °C min^{-1}) for 4 h. The specific surface area was evaluated by the BET method[66] using adsorption data in the range of relative pressure from p/p_0 = 0.05 to p/p_0 = 0.25. The *t*-plot method[67] was applied to determine the volume of micropores (V_{mic}). The adsorbed amount at relative pressure p/p_0 = 0.98 reflects the total adsorption capacity (V_{tot}).

The concentration of Lewis (L) and Brønsted (B) acid sites was determined after adsorption of d_3-acetonitrile (Ac) by FTIR

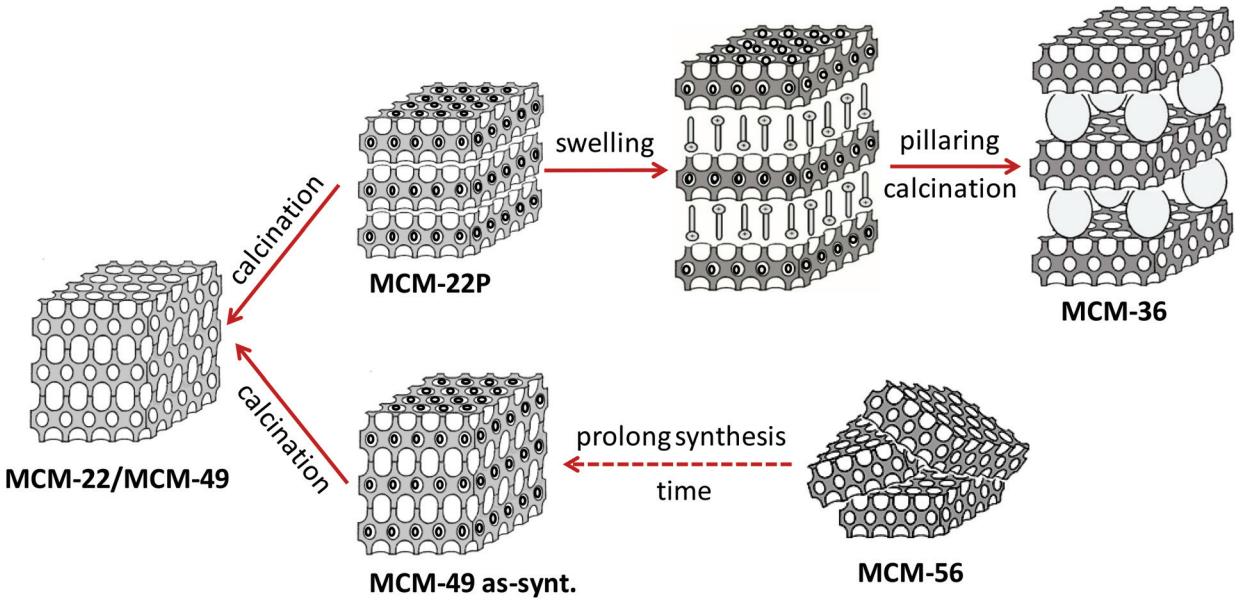

Scheme 1 MWW family presented by MCM-22P, MCM-49 and MCM-56 prepared by direct synthesis and MCM-36 prepared by post-synthetic modification of MCM-22P. The red dot-line presents the assumed transformation of delaminated form MCM-56 into regular 3D MCM-49 if the synthesis time is prolonged.

spectroscopy on a Nicolet Protégé 460 Magna with a transmission DTGS and MTC/A detector. Zeolites were pressed into self-supporting wafers with a density of 8.0–12.0 mg cm^{-2} and activated *in situ* at 450 °C overnight. Before adsorption d_3-acetonitrile was degassed by freezing and thawing cycles. d_3-Acetonitrile was adsorbed at ambient temperature for 30 min at a partial pressure of 900 Pa, followed by desorption for 20 min. All spectra were recorded with a resolution of 4 cm^{-1} by collecting 128 scans for a single spectrum at room temperature. The experimental data were recalculated to a normalized wafer (density of 10 mg cm^{-2}). The concentrations of Lewis and Brønsted acid sites were evaluated from the integral intensities of bands at 2323 cm^{-1} (Lewis acid sites) and at 2294 cm^{-1} (Brønsted acid sites) using extinction coefficients ε (L) = 3.6 cm μmol^{-1} and ε (B) = 2.05 cm μmol^{-1}.[68]

The presented IR spectra both for d_3-acetonitrile and for 2,6-di-*tert*-butyl-pyridine (DTBP) are not correlated to the standard mass. A large probe molecule DTBP was used to determine the concentration of acid sites located on the external surface of zeolites.[69] The adsorption of DTBP was performed at 150 °C at equilibrium probe vapor pressure with the zeolite wafer for 15 min. Desorption proceeded at the same temperature for 1 h followed by collection of spectra at room temperature.

The size and shape of zeolite crystals were examined by scanning electron microscopy (SEM, JEOL, JSM-5500LV). For the measurement, crystals were coated with a thin platinum layer by sputtering in the vacuum chamber of a BAL-TEC SCD-050.

Thermogravimetric analysis of the zeolite catalysts was performed using a TA Instruments TGA Discovery series equipment and operating at a heating ramp of 10 °C min^{-1} from room temperature to 900 °C under the flow of nitrogen (20 mL min^{-1}, Linde 3.0). Approximately15 mg of sample was heated in an open alumina crucible.

2.3. Reaction studies

The properties of zeolite samples were investigated in aldol condensation of furfural and acetone. The catalytic experiments were carried out in a 200 ml stirred batch reactor (Parr autoclave) at 100 °C. Before the start of the catalytic runs, 0.5 g of catalyst was mixed together with a mixture of 19.75 g of acetone and 3.25 g of furfural (acetone/furfural molar ratio 10/1) and loaded into the autoclave. After initiation of the heating the desired temperature was achieved in ~60 min, and the autoclave was kept at T = 100 °C for an additional 0, 2 or 4 h.

Analysis of the reaction products was performed on an Agilent 7890A GC unit equipped with a flame ionization detector using a HP-5 capillary column (30 m/0.32 ID/0.25 μm). The obtained products were identified based on the standard reference compounds. Catalytic activity is expressed in terms of conversion, which is defined as the fraction of furfural which has reacted. Selectivity was calculated by dividing the percentage of furfural moles presented in the products by total moles of converted furfural.

3. Results and discussion

3.1. Catalyst characterization

3.1.1. XRD. XRD patterns of the MWW materials are depicted in Fig. 1. Although all the prepared materials possess the same MWW topology of the layers, the differences in the layer arrangement can be recognized on the basis of XRD pat-

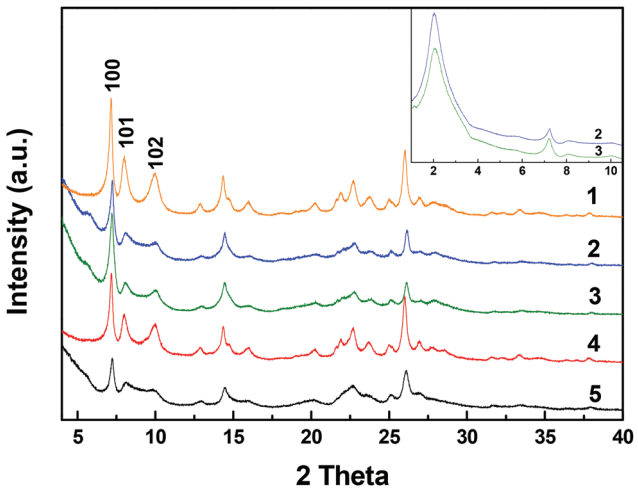

Fig. 1 XRD patterns of MWW samples. (1) MCM-22, (2) MCM-36(1), (3) MCM-36(2), (4) MCM-49, (5) MCM-56.

terns. The XRD patterns of MCM-22 and MCM-49, as the three-dimensional zeolites, differ from the others and show three well-defined peaks corresponding to (100) (2θ = 7.1–7.2°), (101) ($2\theta \approx 8°$) and (102) ($2\theta \approx 10°$) reflections, which is in good agreement with previous reports[70] and proves good crystallinity and phase purity of these materials. In contrast, the two-dimensional MWM forms (MCM-56 and MCM-36) have a broad band between 8° and 10° indicating the disappearance of atomic order in the third dimension, along the *c*-axis. In addition, both MCM-36 samples are distinctly characterized by a high intensity low angle peak around ≈2 °C, corresponding to a *d*-spacing of about 5 nm. It corresponds well to an idea of MWW layers of *ca.* 2.5 nm thick separated by around 2.5 nm interlayer space filled partially with amorphous silica pillars.[53] Similarly, in MCM-56 the broad band between 8° and 10° indicates that the material is composed of thin layers that extend in the *a* and *b* directions with a lack of order in the *c*-axis direction.[63] As the intermediate to MCM-49, delaminated MCM-56 is not fully crystalline and an amorphous part is most probably present evaluated from lower intensities of diffraction lines in comparison to fully crystalline MCM-49. Based on the analysis of XRD patterns it can be concluded that a series of materials with MWW topology differing in layer arrangement was prepared in the pure phase (with the exception of MCM-56, which has an amorphous part present).

3.1.2. SEM. Fig. 2 shows SEM images of the MWW materials. The morphology of the individual crystals of all materials shows a thin plate-like shape that is a characteristic of MWW. The samples differ somewhat with regard to the size of individual crystals and their aggregation. The crystal size can be influenced by the synthesis time as is demonstrated on the row MCM-22 (96 hours) ≥ MCM-49 (93 hours) > MCM-56 (33 hours, the intermediate to MCM-49). The individual crystals of MCM-22, MCM-49 and MCM-56 have a length of 0.2–0.5 μm and a thickness of about 0.1 μm. In the case of MCM-36 materials the aggregation of individual crystals is visible as they underwent swelling and pillaring treatments under relatively severe conditions. In the case of MCM-36 the length of crystals is about 1 μm. It was pointed out that the large crystals of MCM-36 might have been previously hidden in the aggregates and became visible only upon swelling and pillaring treatments.[70]

3.1.3. N_2 adsorption. The textural parameters of the prepared MWW materials were evaluated based on nitrogen isotherms (Fig. 3(A)). MCM-22 and MCM-49 zeolites have very similar isotherms typical of microporous materials according to the IUPAC classification.[71] It was mentioned above that MCM-22 and MCM-49 crystallize as aggregates of thin sheets. As a result we observe a narrow hysteresis loop at higher relative pressure in both zeolites corresponding to nitrogen condensation in interlayer voids of the aggregates. The BET surface areas for MCM-22 and MCM-49 are similar, 505 and 455 $m^2\ g^{-1}$, as well as the micropore volumes, 0.151 and 0.165 $cm^3\ g^{-1}$, respectively (for more details see Table 2). Delaminated MCM-56 has the nitrogen isotherm with a distinctive hysteresis loop corresponding to the adsorption in the interlayer space of delaminated MWW layers. As MCM-56 is the intermediate to MCM-49 and cannot be fully crystalline (discussion *vide supra*), also the BET surface area is lower in comparison to MCM-49, 401 *vs.* 455 $m^2\ g^{-1}$. Nevertheless, both materials differ noticeably in the micropore and total volume when the micropore volume for MCM-56 and MCM-49 is 0.113 and 0.165 $cm^3\ g^{-1}$ and the total pore volume 0.701 and 0.459 $cm^3\ g^{-1}$, respectively (see Table 2). The higher micropore volume in MCM-49 is caused by the presence of the regular three-dimensional framework with a 10-ring two-dimensional channel system and the presence of supercages. On the other hand, in MCM-56 the supercages were not formed as the layers are not condensed and irregularly aggregated. The layers are expected to be connected only by hydrogen bonds. The pillared materials MCM-36 possess isotherms with a gradual increase in the adsorbed amount in the relative pressure range p/p_0 0.01–0.3. It is typical of mesopore materials with the mesopore size below 4 nm.[72] Also the high surface areas for both MCM-36 materials, 606–762 $m^2\ g^{-1}$, indicate the formation of a new mesopore structure. The micropore volumes decreased in comparison to MCM-22, 0.062–0.097 $cm^3\ g^{-1}$. This is related to the presence of amorphous silica pillars, which form a considerable part of the material. Alike MCM-56, in MCM-36 materials supercages were not formed and MWW layers have only large cups on the surface and 10-sinusoidal channel system inside the layers. The mesopore size distribution of pillared MCM-36 (1) and (2) materials (displayed in Fig. 3(B)) is centered at 2.3 and 2.5 nm, nicely corresponding to the data determined from XRD patterns (see section 3.1.1).

The type of obtained isotherms reflects the structural differences between the samples. Thus, isotherms of MCM-22 and MCM-49 with the same structural characteristics are very close to those typical of microporous solids,[73] showing a fast increase in the adsorbed amount occurring at very low p/p_0, followed by long almost horizontal plateau extending up to the high p/p_0 values. A very narrow hysteresis loop observed for these samples at high p/p_0 values indicates the presence of

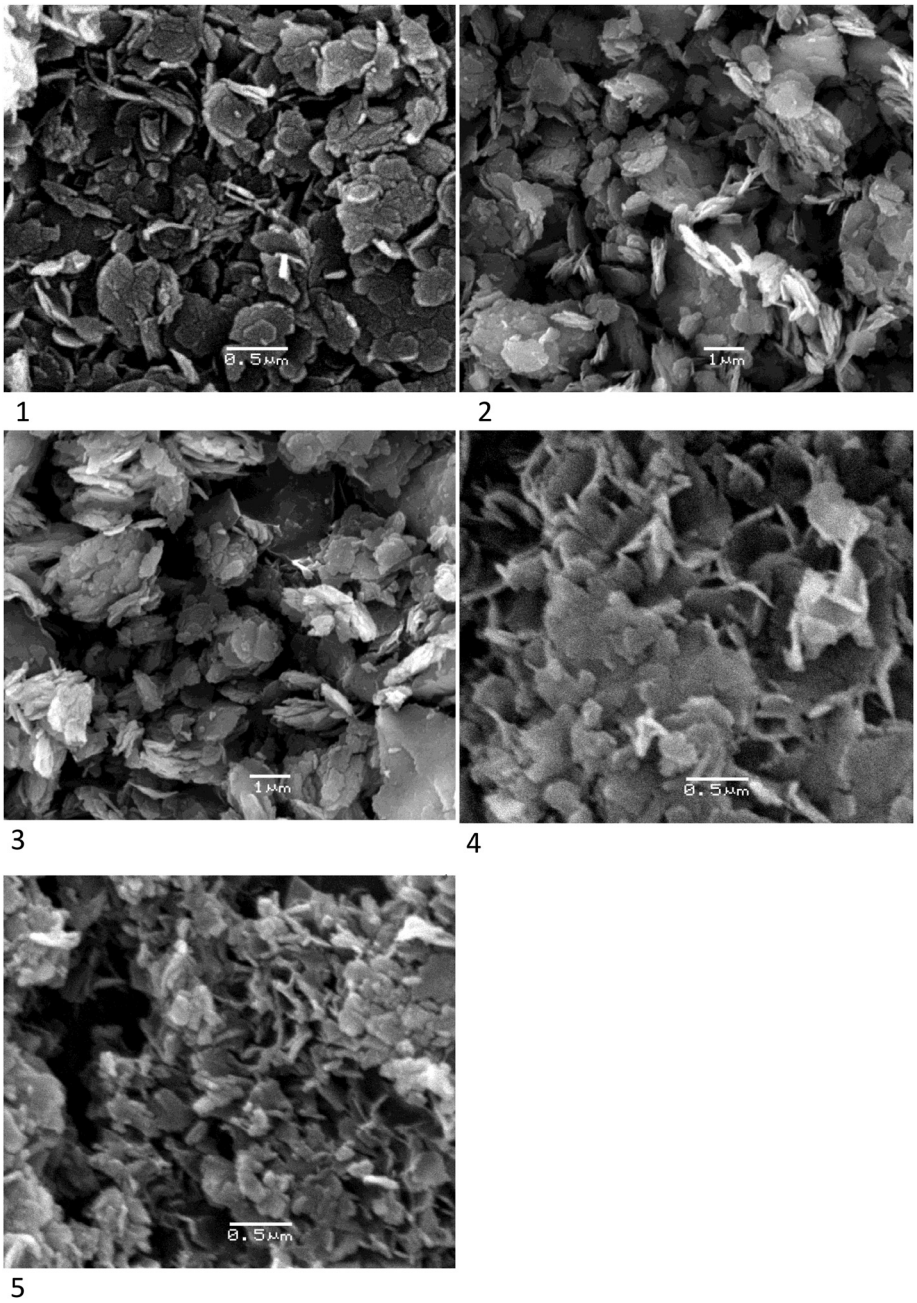

Fig. 2 SEM images of zeolites samples. (1) MCM-22, (2) MCM-36(1), (3) MCM-36(2), (4) MCM-49, (5) MCM-56.

some slit-shaped, wide mesopores (or narrow macropores) or platelet particles,[73] most probably originating from the aggregation of the lamellar particles.

A change in the shape of the isotherms for two MCM-36 samples reflects the structural changes in these materials caused by the swelling followed by pillaring. The marked increase in the adsorption capacity of MCM-36 up to p/p_0 = 0.3–0.4 evidences capillary condensation and indicates the presence of mesopores created by pillaring. At higher p/p_0 there is a clear hysteresis loop of type H4 characteristic of layered materials.[74,75]

In comparison with MCM-22, the isotherm of MCM-56 shows a slightly lower N_2 adsorption amount at p/p_0 = 0–0.6. It proves a slight decrease in the amount of micropores in this sample due to the absence of bonding between "MCM-22 monolayers". In higher p/p_0 region of the N_2 isotherm the adsorption amount increases very fast due to a well-developed interlamellar space formed by MCM-22 sheets arrayed in a disordered manner forming the so-called partially delaminated structure.[63,76]

The values of the calculated specific surface areas and total pore volumes are summarized in Table 2.

All the prepared samples possess high BET area. The observed differences in BET area between the samples are in full agreement with their structural features. The smallest BET

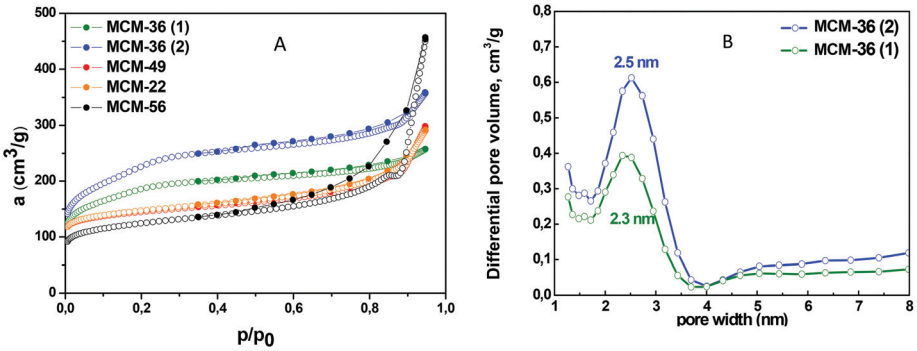

Fig. 3 (A) Nitrogen isotherms of the investigated MWW materials. Open circles – adsorption branch, closed circles – desorption branch. (B) The mesopore size distribution for pillared MCM-36 materials.

Table 2 Textural properties of MWW materials determined from nitrogen adsorption measured at 77 K

Sample	BET ($m^2\ g^{-1}$)	S_{ext} ($m^2\ g^{-1}$)	V_{mic} ($cm^3\ g^{-1}$)	V_{tot} ($cm^3\ g^{-1}$)
H-MCM-22	505	176	0.151	0.449
H-MCM-36(1)	762	656	0.062	0.553
H-MCM-36(2)	606	430	0.097	0.398
H-MCM-49	455	134	0.165	0.459
H-MCM-56	401	181	0.113	0.701
H-BEA(25)	608	222	0.174	1.017

BET – specific surface area (from the BET method). V_{mic} – micropore volume (from the *t*-plot method). V_{tot} – total pore volume at $p/p_0 = 0.97$.

area (401 $m^2\ g^{-1}$) is observed for delaminated MCM-56 sample representing a disordered agglomeration of MCM-22 monolayers without in-registry alignment in the *c* direction with no interlayer links. For MCM-22 and MCM-49 samples the BET area increases to 505 and 455 $m^2\ g^{-1}$, respectively, due to the ordering of "MCM-22 monolayers" in the vertical direction resulting in the formation of a three-dimensional crystalline framework and creation of 12-ring supercages between the layers. The further growth of the *c* parameter of the crystalline framework due to the introduction of the silica pillars not only influences the BET area, but also results in a substantial increase of the external surface area for both MCM-36 samples (Table 2).

The largest volume of micropores is observed for MCM-22 and MCM-49 samples as their pore system consists of "MWW monolayers" and large cylindrical supercages between them. It is obvious that delaminated materials not having supercages and channels connecting them have lower micropore volume regardless of whether the layers remain disordered (MCM-56) or connected by siliceous pillars (MCM-36). At the same time, the disordered arrangement of "MWW monolayers" in MCM-56 generates significant inner mesoporosity in this sample. It was shown[76,77] that pillaring may also result in the formation of mesopores. However, according to ref. 77, the volume of the formed mesopores depends on the pillaring procedure. Hence, it is not surprising that the two MCM-36 samples studied here have different mesopore volumes; MCM-36(1) exhibits considerably larger mesopore volume in comparison with MCM-36(2) (Table 2). Taking into account the difference in Si/Al ratio in the reaction mixture for the preparation of these samples (Table 1), it may be assumed that the mesopore volume of the final MCM-36 materials is determined not only by the pillaring procedure, but also by the properties of the intermediate MCM-22P material.

Table 2 also shows that the BET area of BEA used as a reference sample differs only slightly from the values determined for MWW samples. However, the BEA sample has a significantly higher V_{tot} due to the well-developed mesoporosity of this material.

3.1.4. Acidity. IR spectra of MCM-22, MCM-36, MCM-49 and MCM-56 in the region of OH stretching vibration are shown in Fig. 4. The well expressed absorption band at 3745 cm^{-1} is assigned to the terminal silanol groups exposed at the external surface. This band is the most intensive for two MCM-36 samples compared with MCM-22 and MCM-49 which can be explained by the presence of silicate pillars in the structure and the increased access to the MWW sheets, *i.e.* increased external specific surface area as indicated also by the nitrogen physisorption results (Table 2). Similarly, the rela-

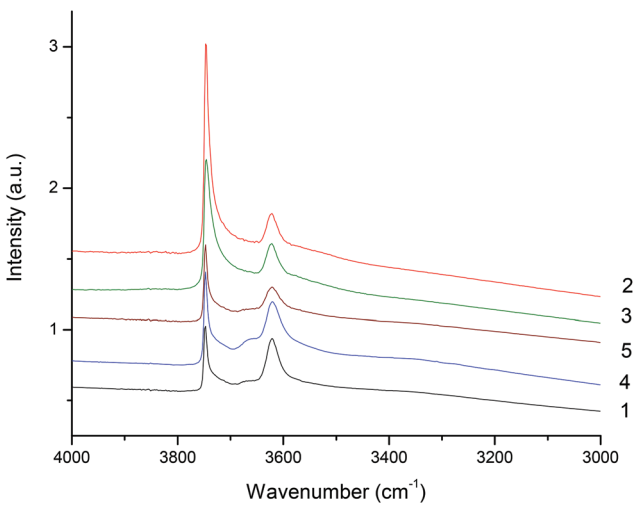

Fig. 4 Region of OH stretching vibration of the studied zeolites. (1) MCM-22, (2) MCM-36(1), (3) MCM-36(2), (4) MCM-49, (5) MCM-56.

tively low intensive band for Si–OH groups in MCM-56 material correlates well with the low external surface area and also the fact that MCM-56 is not a fully crystalline material (discussion *vide supra*) (Table 2).

The band at 3620 cm^{-1} is attributed to the acidic bridging Si(OH)Al hydroxyls associated with the framework Al. The intensity of this band is the highest for MCM-22 and MCM-49 due to a high structural ordering of these zeolites. It is also seen that both delamination (MCM-56) and pillaring (MCM-36) result in a partial degradation of the Brønsted acid centers. This is in accordance with previous results.[64,78] The difference between the two MCM-36 samples should be also noted. The intensity of the band at 3620 cm^{-1} is slightly lower for MCM-36(1) in comparison with MCM-36(2). Fig. 4 also shows that spectra of OH-groups of MCM-22, MCM-49 and MCM-56 contain a very weak band between 3660 and 3670 cm^{-1}, which is characteristic of OH groups located on extra-framework aluminum (EFAL) centers.[79] It was suggested that some of these aluminum-containing species may have rather strong Brønsted-type acidity.[80]

It is generally accepted that acid sites in the MWW family materials can have in principle three different locations depending on packing arrangement of "MWW monolayers".[62] For delaminated MCM-56 these centers can be present in the sinusoidal 10-ring channels and in cups located on the external surface of the crystals. In addition to these two possible locations, MCM-22 and MCM-49 also contain acid sites in large supercages formed by condensation of "MWW monolayers" that are accessible by another network of 10-ring pores. Similarly to MCM-56, MCM-36 material does not contain large supercages. However, it can be expected that the pillaring procedure can also result in a decrease of accessibility to acid sites located in the cups due to their blocking by the silicate pillars.

Small basic molecules, such as pyridine or d_3-acetonitrile, can easily enter the 10-ring channels of zeolites and can be used as probes for acid sites located inside supercages and the 2D sinusoidal pore system of MWW family materials. Conversely, large basic molecules, such as 2,6-di-*tert*-butyl-pyridine (DTBP) cannot enter the 10-ring, so they are adsorbed only on the Brønsted acid sites located on the external surface of such zeolitic materials.[69] Thus, DTBP was used to determine the concentration of the external acid sites of the prepared MWW materials, while the total concentration of Brønsted and Lewis acid sites, respectively, was evaluated by FTIR of the adsorbed d_3-acetonitrile (Ac).

The concentrations of acid sites in the studied zeolites determined with both probing molecules, Ac and DTBP, is presented in Table 3. It can be seen that the highest concentration of Brønsted acid sites (BAS), 0.335 mmol g^{-1} and 0.317 mmol g^{-1}, is observed for three-dimensional MWW zeolites with the largest micropores volume, MCM-22 and MCM-49, respectively. It is in good agreement with the high intensity of the band of bridged OH-groups at 3620 cm^{-1} for these samples (Fig. 4). The concentration of BAS in MCM-36 and MCM-56 is lower, which is in line with the lower intensity of the band at 3620 cm^{-1}. The lower concentrations of BAS in MCM-36 can be explained by the presence of silica pillars, which generally dilute the concentrations of active sites. It was already mentioned above that MCM-56 is not fully crystalline and it is also reflected in its acidity. Since the MCM-36 materials were prepared from MCM-22P precursors differing in Si/Al ratio, it is reasonable that the final pillared MCM-36 also differ in the acid site concentrations. It should be additionally noted that MCM-49 and MCM-56 possess an increased concentration of Lewis acid sites (LAS), which is most probably a consequence of their higher Al content in comparison with MCM-22 and MCM-36 materials.

Table 3 Acidic properties of the samples determined by FTIR using d-acetonitrile and DTBP as probe molecules

Sample	C_B (DTBP) (mmol g^{-1})	C_B (Ac) (mmol g^{-1})	C_L (Ac) (mmol g^{-1})	Si/Al (Ac)[b]
H-MCM-22	0.044	0.335	0.247	19.1
H-MCM-36(1)	0.067	0.196	0.177	29
H-MCM-36(2)	0.053	0.249	0.245	21.6
H-MCM-49	0.036	0.317	0.537	11
H-MCM-56	0.050	0.210	0.380	16
H-BEA[a]	0.125	0.353	0.220	—

[a] Concentration of acid sites in BEA zeolite was determined by pyridine-FTIR. [b] Calculated from the Ac adsorption data.

The concentration of external Brønsted acid sites determined by DTBP-FTIR reflects differences in structural features of the investigated MWW materials. The largest concentration of the external BAS is observed for MCM-36 and MCM-56, which correlates with their larger external surface and the increased concentration of large cups exposed to the outside and hence the improved accessibility of acid sites. Similarly, the lower concentration of external BAS in MCM-22 and MCM-49 is due to their lower external surface area and thus less cups per gram of catalyst.

Table 3 also shows that the reference BEA sample possesses a relatively high concentration of BAS, both total and those located on the external surface, 0.353 and 0.125 mmol g^{-1}, respectively, which is a consequence of high aluminum content and its good textural characteristics (Table 2). Besides, the high concentration of acid sites in BEA determined by DTBP-FTIR can be partially attributed to the penetration of DTBP into the pores of BEA and its interaction with both external and internal Brønsted acid sites.[69]

3.2. Catalyst performance

3.2.1. Conversion and selectivity. It was shown in ref. 52 that consecutive interaction of furfural and acetone over acidic and basic catalysts results in the formation of the following main products: FAc (produced by dehydration of an intermediate alcohol) and F_2Ac (Scheme 2). A distinctive feature of this reaction over zeolites is the formation of an additional reaction product, $(FAc)_2$, which is formed by dimerization of FAc, *i.e.* it is not a direct aldol condensation product. Additionally, self-condensation of acetone also takes place to a small extent

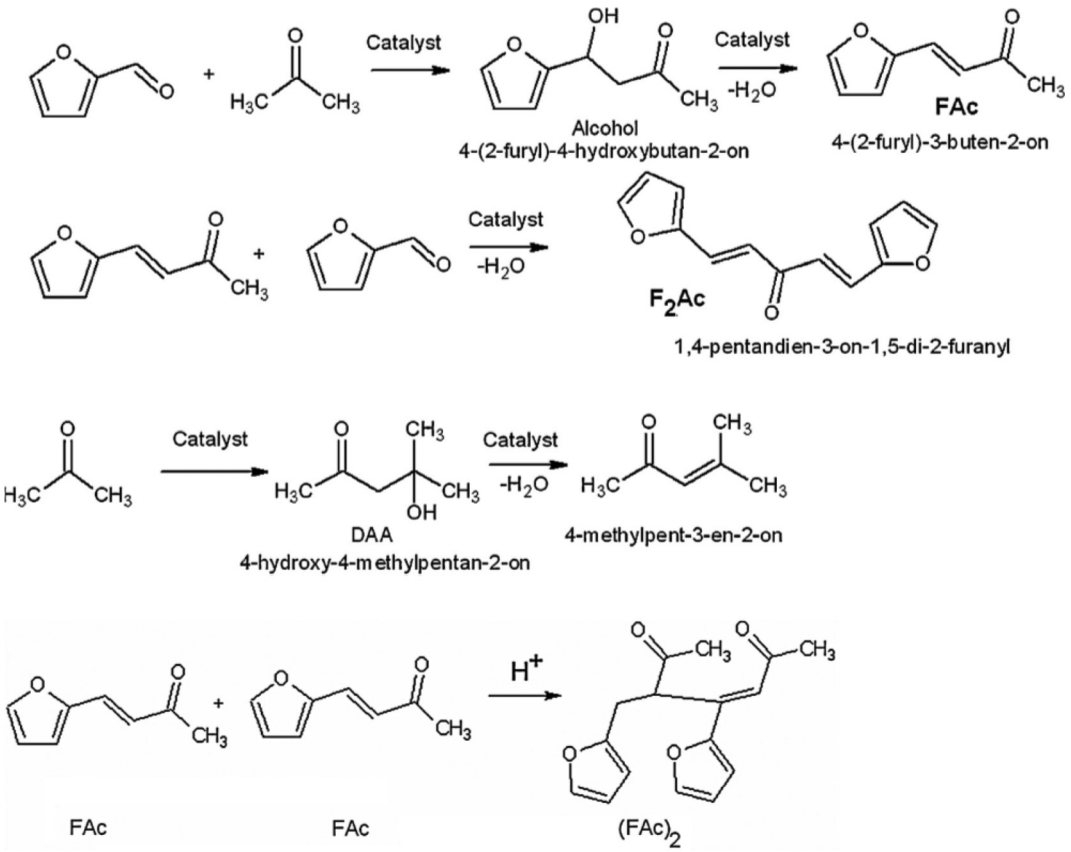

Scheme 2 Aldol condensation between furfural and acetone over acidic catalysts.[52]

leading to diacetone alcohol (DAA) that is subsequently dehydrated and affords mesityl oxide (Scheme 2).

Furfural conversion over MWW materials in aldol condensation of furfural and acetone is depicted in Fig. 5 and 6. Fig. 5(A) shows furfural conversion obtained over different catalysts after 2 hours of the reaction. It is seen that the activity of all MWW samples is higher than the activity of BEA zeolite which was used as the reference sample. It can be concluded that MWW materials exhibit better activity than the other zeolites investigated so far for the aldol condensation of furfural and acetone as the following activity sequence was reported previously: BEA > FAU > MOR > MFI.[52] Considering the high BET area and acidity of the reference BEA sample, this might be surprising and indicates that other factors, such as the specific structural features of MWW materials, play an important role. Among the MWW samples, MCM-22 was the most active in aldol condensation with furfural conversion of 60% after 2 hours of the reaction. The conversion of furfural over MCM-49 and MCM-56 was only slightly lower being 55 and 52%, respectively, after 2 hours. Finally, the lowest conversion of 30 and 35% was obtained over MCM-36(2) and MCM-36(1), respectively, *i.e.* the pillared materials. It can be concluded that introduction of silicate pillars between the "MWW monolayers" resulted in deterioration of the catalytic properties of

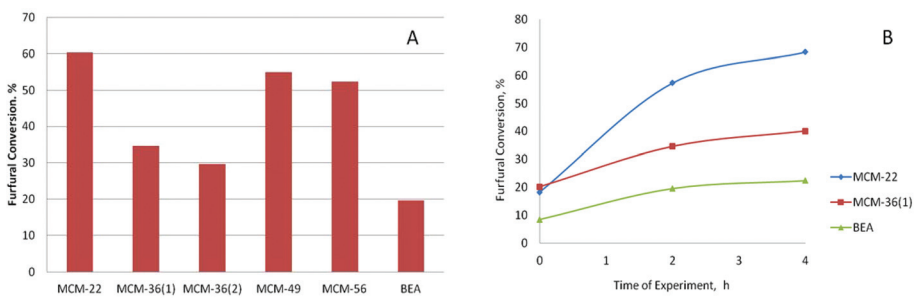

Fig. 5 (A) Furfural conversion obtained on different catalysts after 2 hours of the reaction at 100 °C and autogenous pressure. (B) Dependence of furfural conversion on the duration of reaction at 100 °C and autogenous pressure.

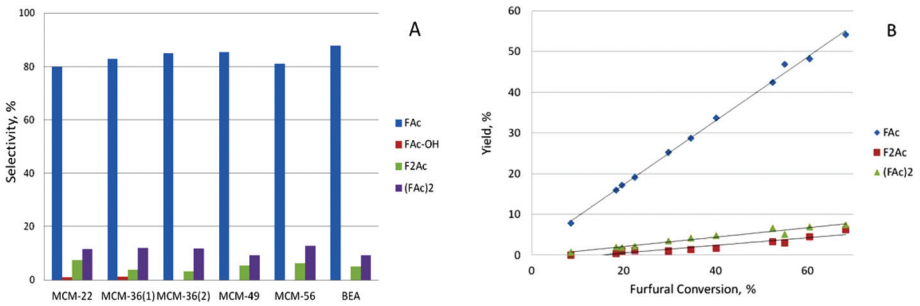

Fig. 6 (A) Selectivity towards the main reaction products in aldol condensation of furfural and acetone over different catalysts after 2 hours at 100 °C and autogenous pressure. (B) Dependence of the yield of reaction products on furfural conversion for all studied MWW samples at 100 °C and autogenous pressure and reaction time from 0 to 4 hours.

these materials in aldol condensation. This is quite surprising, taking into account the larger external surface and better accessibility of acid sites which can be deduced from the DTBP-FTIR results according to which the concentration of the external BAS is 20–50% larger in MCM-36 than in MCM-22. Moreover, increased activity of MCM-36 as compared with MCM-22 was reported for a number of organic reactions.[64,78,81] Additional insight can be obtained when looking at the time dependence of furfural conversion. Fig. 5(B) shows that at $t_{reac.} = 0$ (*i.e.* when reaching $T = 100$ °C inside the batch stirred reactor, which takes about 1 hour) the furfural conversion over MCM-36(1) is slightly higher than over MCM-22 catalyst, 20 *vs.* 18%. When analyzing the shape of the conversion as a function of time curve it can be evidenced that the reaction rate over MCM-22 exceeds that observed for MCM-36(1) and BEA. This is a clear indication of catalyst deactivation that was reported also previously for this reaction system.[52] The aspect of coke formation in these zeolites and its impact on catalyst performance will be discussed in the present article.

Apart from furfural conversion, selectivity towards the main products is an important parameter of the overall catalyst evaluation. The selectivity data are summarized for all investigated catalysts after 2 hours of the reaction (Fig. 6(A)). Generally, the composition of the reaction products obtained over MWW samples corresponds to that observed for zeolites with different structural types.[52] For all the catalysts in the present study FAc is the main reaction product formed with selectivity ≥80%. In accordance with the generally accepted reaction network, this compound is formed on acidic sites by dehydration of the corresponding alcohol, FAc–OH.[52] Other reaction products include F_2Ac formed by condensation of a furfural molecule with FAc as well as $(FAc)_2$. It was shown in ref. 52 that the latter compound is a result of dimerization of two (olefinic) FAc molecules. Apparently, the formation of this dimer is a distinctive feature of aldol condensation of furfural and acetone carried out in the presence of acidic catalysts as this product was not observed when hydrotalcites, *i.e.* basic catalysts, were used.[33] The yields of FAc, F_2Ac and $(FAc)_2$, respectively, increased linearly with the growth of furfural conversion (Fig. 6(B)) with no obvious dependence on the structural features of the studied catalysts. The obtained results confirm that aldol condensation of furfural and acetone over acidic catalysts takes place as one and the same sequence of successive transformations, and furfural conversion is kinetically governed and no molecular sieving effect is observed. This could mean that at least the secondary reactions proceed on the external surface. However, when comparing the concentration of the external BAS with the observed conversion (Table 3, Fig. 5), they do not correlate. In fact, the conversion after 2 hours appears to decrease with increasing concentration of external Brønsted acid sites, *i.e.* those determined by DTBP-FTIR (Table 3). This suggests that some of the reactions might proceed at the internal surface that is significantly larger in the case of MCM-22 and MCM-49 (Table 2) that also exhibit higher conversion than both MCM-36 catalysts.

It was shown in ref. 52 that the conversion over large-pore three-dimensional zeolites in aldol condensation of furfural and acetone is considerably higher compared with medium-pore three-dimensional or wide-pore mono-dimensional materials. This has been attributed to the constrained space within MFI and MOR pores for the formation of aldol condensation products. Consequently, the observed, though very low conversion, over MFI and MOR was attributed to the activity of the external acid sites.[52] From this point of view, it is hard to believe that the sinusoidal 10-ring channels of MWW materials could be responsible for the high activity of these materials in aldol condensation, which is even higher than that of BEA zeolite, while MFI was virtually inactive although its 10-ring pores are slightly larger than those of MWW materials (MFI, 5.3 × 5.6 and 5.1 × 5.5 Å *vs.* MWW, 5.1 × 4.1 and 5.5 × 4.0 Å). This points to the conclusion that apart from the external surface acid sites, the acid sites located in the supercages of MWW are of great importance for catalytic transformations. Considering the dimensions of acetone and furfural, 4.1 × 2.4 × 2.7 Å and 5.2 × 3.5 × 1.7 Å, these molecules can reach the supercages of MWW through the 10-ring pores, where they could form the first aldol condensation product, FAc (8.9 × 3.6 × 2.2 Å), while the formation of the second aldol condensation product, F_2Ac (13.3 × 5.3 × 1.9 Å), in the supercages is highly unlikely. Since FAc is a rather flat molecule it might be able to diffuse out from the supercages through the 10-ring channels. In contrast, the intersections of the 10-ring pores in MFI may

not accommodate even FAc, which would explain the very low activity of MFI reported earlier.[52] More importantly, it can help explain the significantly higher conversion over MCM-22 and MCM-49 in comparison with MCM-36 catalysts that possess only cups at the external surface, but no supercages. This conclusion is supported by the catalytic performance of the two MCM-36 catalysts, where MCM-36(1) shows higher activity than MCM-36(2) despite having lower total concentration of acid sites (Table 3) but higher concentration of surface acid sites. It proves that the interaction of furfural and acetone over these samples generally takes place in the large cups of the external surface of crystallites.

In lamellar MCM-56, the concentration of acidic centers determined by DTBP-FTIR is also slightly lower than that in MCM-36(2) (0.50 *vs.* 0.53 mmol g^{-1}), but its activity in aldol condensation is close to that of MCM-22 and MCM-49 (Fig. 5). MCM-56 is an intermediate crystalline product in the MCM-49 synthesis: the increase of crystallization time results in the condensation of the lamellar monolayers of MCM-56 into the three-dimensional MCM-49 framework. It could be assumed that the MCM-56 sample may contain a small admixture of condensed MCM-49, which is confirmed by the splitting of the XRD reflection at 2θ = 8–10°. In that case there should be available supercages and the observed MCM-56 activity would be higher than what would be expected solely on the basis of the concentration of acid sites determined by DTBP-FTIR.

Taking into account the structural features of MWW materials, an assumption could be made that their catalytic activity may be considerably influenced by the location and concentration of Brønsted acid sites. Nevertheless, with respect to Lewis acid sites the situation is not as clear. Comparing the acidic properties of the samples (Table 3) with their activity in furfural conversion (Fig. 5) it can be concluded that the catalytic properties of MWW materials show poor correlation with the concentration of Lewis acid sites. This observation is in total agreement with our results obtained for different zeolites used as catalysts in aldol condensation.[52] However, there is not yet enough information available to make a definitive conclusion about the role of Lewis acid sites both in the transformation of the feed molecules and in coke formation. Apparently, a comprehensive understanding of the impact of various acid sites is possible only after an additional study of a series of molecular sieve samples having the same structure but different Brønsted/Lewis acid sites ratios.

3.2.2. Deactivation of catalysts. Based on the conversion time dependence, it has been concluded that the activity of MWW materials in aldol condensation continuously decreases with increasing length of the experiment (Fig. 5B). All the catalysts after reaction are black in color suggesting that they have accumulated a significant amount of carbonaceous deposits (coke). Hence, after thorough washing with acetone, the samples were studied by TGA/DTG to evaluate the content and possibly also the distribution of carbonaceous deposits on the spent catalysts.

Two regions of weight loss, low-temperature (LT) and high-temperature (HT), are observed on DTG curves (Fig. 7). The LT region consists of two peaks, at 70–80 °C and 140–150 °C corresponding to the residual organic substances (acetone, ethanol, furfural, mesityl oxide) and water removal. The weight loss at this stage is equal to 4.4–6.4% for all the samples. The position and intensity of the DTG peaks located in the HT region show rather poor dependence on structural features of MWW. Nevertheless, several conclusions can be made. Clearly distinguishable peaks with maxima at 320–340 °C and 507–563 °C are observed on the DTG curves of all samples. Since MWW materials have a dual pore system, it could be assumed that the two peaks on the DTG curve correspond to the removal of coke from large cups on the external surface of the zeolite crystals (T = 320–340 °C) and from the 10-ring sinusoidal channels (T = 507–563 °C). The determined weight loss associated with each of these peaks is in line with this assumption. The largest weight loss in the range of T = 320–340 °C is observed for MCM-36 and MCM-56 samples (Table 4) with

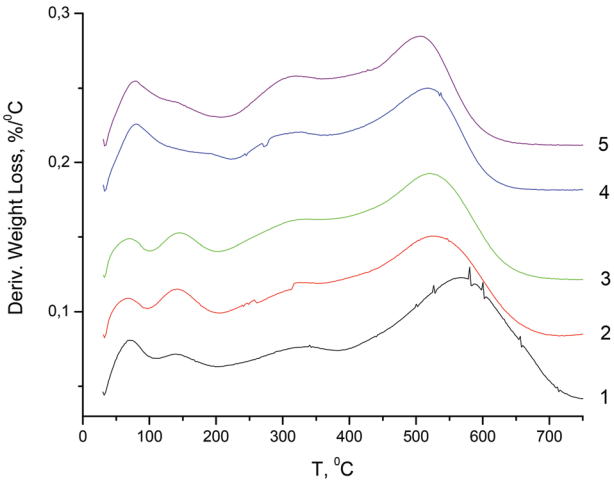

Fig. 7 DTG profiles of spent MWW materials obtained in oxidative atmosphere (air). (1) MCM-22, (2) MCM-36(1), (3) MCM-36(2), (4) MCM-49, (5) MCM-56.

Table 4 Results of TGA for MWW zeolite samples carried out under oxidative (oxygen) atmospheres

Sample	Temperature region (°C)	Maximum value on DTG curve (°C)	Weight loss (%)
MCM-22	20–200	72; 145	5.0
	200–750	331	6.0
		563	17.4
MCM-36(1)	20–200	72; 144	4.6
	200–750	341	7.3
		526	12.5
MCM-36(2)	20–200	72; 146	4.4
	200–750	334	7.6
		521	12.1
MCM-49	20–200	72; 170	6.4
	200–750	332	5.3
		521	11.8
MCM-56	20–200	72; 151	6.2
	200–750	320	7.8
		507	10.8

easily accessible external large cups due to the delamination and pillaring. On the other hand, MCM-22 with a well-developed microporosity (Table 2) has the highest weight loss at $T \approx 560$ °C (17.4%). However, the MCM-49 sample with crystal structure and value of micropore volume similar to those of MCM-22 appears to be an exception from these considerations. Taking into account the high concentration of LAS in MCM-49 (Table 3), it may be assumed that these active sites could be inactive or less active in coke formation on the MCM-49 crystals.

3.2.3. Conversion and selectivity over coked samples. To evaluate the influence of carbonaceous deposits on the catalytic properties of MWW materials, the catalyst samples after reaction were separated from the organic phase, washed with excess of ethanol, dried at 120 °C for 12 hours and re-used in the aldol condensation under the same reaction conditions. The results are presented in Table 5.

It is seen that furfural conversion over both re-used MCM-36 samples decreased drastically to about 5–7% from about 30–35% obtained over the fresh catalysts (Table 5). At the same time, the conversion of furfural over re-used MCM-22 and MCM-49 samples decreased only to 33–38% from the original 55–60% conversion of furfural. The results suggest that rapid formation of carbonaceous deposits which are poorly soluble in ethanol occurs in the cups located both on the external surface of MWW monolayers and in the mesoporous pillared space between these layers. On the other hand, in MCM-22 and MCM-49 possessing large supercages, the coking rate and growth of the carbonaceous deposits are limited, which makes it possible to remove such carbonaceous deposits from supercages by a simple washing with ethanol. Taking into account the structural differences between condensed and laminated/pillared MWW materials it can be assumed that the main reason for the different catalytic properties of the studied samples MWW is concerned with the presence of supercages located between "MWW monolayers" which are accessible through 10-ring pores.

It follows that the presence of cups on the surface of "MWW monolayers" or supercages (double cups) in the structure of MWW materials introduces a positive impact on the aldol condensation activity of these materials in comparison with conventional microporous crystalline materials, zeolites, as it is apparent from the comparison with the reference sample, a wide-pore three-dimensional BEA sample.

Table 5 Comparison of catalytic properties of fresh and used MWW materials. T = 100 °C, t = 2 hours, autogenous pressure

Sample	Furfural conversion (%)	Selectivity[a] (%)		
		FAc	F_2Ac	$(FAc)_2$
MCM-22	60.4	82.1	6.7	11.5
MCM-22-coked	33.0	91.7	3.5	4.8
MCM-36(1)	34.6	83.7	3.2	13.1
MCM-36(1)-coked	5.6	100	0	0
MCM-36(2)	29.7	84.8	2.8	12.4
MCM-36(1)-coked	7	94.9	0	5.1
MCM-49	55.0	85.4	5.4	9.2
MCM-49-coked	37.6	92.5	2.9	4.5

[a] FAc–OH was not observed among the reaction products.

4. Conclusions

A number of MWW materials (MCM-22, MCM-49, MCM-56 and MCM-36) were used as catalysts for the aldol condensation of furfural and acetone. Their performance was compared to that of large-pore zeolite BEA in a batch reactor at 100 °C, autogenous pressure and a reaction time of 0–4 h. To establish the relationship between the physico-chemical and catalytic properties of these micro/mesoporous materials, the samples were characterized by XRD, SEM, N_2 adsorption, FTIR and TGA. It was found that the acidic solids possessed appreciable activity in the reaction and their use resulted in the formation of products of aldehyde–ketone interaction. Surprisingly, MCM-22 and MCM-49, *i.e.* condensed materials containing supercages, exhibited higher activity than two MCM-36 catalysts having larger accessible external surface area than the condensed materials due to delamination and pillaring. This was explained by the participation of the active sites located in the supercages in the reaction in addition to the active sites present in the cups located on the external surface of MWW materials. Moreover, all MWW family catalysts gave higher conversion than the large-pore zeolite BEA. Nevertheless, furfural conversion decreased rapidly for all catalysts due to coke formation. Unexpectedly, the deactivation was found to be more severe for MCM-36 catalysts than for MCM-22 and MCM-49, which was attributed to the reaction taking place also in supercages that are protected by 10-ring channels from severe coking. In contrast, the cups located on the external surface were coked rapidly which resulted in low conversion over MCM-36 catalysts as well as in a shift in product selectivities. The selectivity to F_2Ac and $(FAc)_2$, *i.e.* products that can be formed due to their dimensions only on the external surface, was lower over coked catalyst than over fresh ones as a result of decreased concentration of the active sites on the external surface.

Acknowledgements

This publication is a result of project no. P106/12/G015 supported by the Czech Science Foundation which is being carried out in the UniCRE centre (CZ.1.05/2.1.00/03.0071) whose infrastructure was supported by the European Regional Development Fund and the state budget of the Czech Republic. The authors are very grateful to Jiří Čejka and Dana Vitvarová, both from the J. Heyrovský Institute of Physical Chemistry, Academy of Sciences of the Czech Republic, for stimulating discussions and FTIR characterization of the catalysts, respectively.

References

1 D. Kubička, I. Kubičková and J. Čejka, *Catal. Rev. Sci. Eng.*, 2013, **55**, 1–78.
2 C. Somerville, H. Youngs, C. Taylor, S. C. Davis and S. P. Long, *Science*, 2010, **329**, 790–792.
3 G. W. Huber and A. Corma, *Angew. Chem., Int. Ed.*, 2007, **46**, 7184–7201.
4 D. L. Klass, *Biomass for Renewable Energy, Fuels and Chemicals*, Academic Press, San Diego, 1998.
5 Y. Sun and J. Cheng, *Bioresour. Technol.*, 2002, **83**, 1–11.
6 X. Hu, L. Wu, Y. Wang, Y. Song, D. Mourant, R. Gunawan, M. Gholizadeh and C.-Z. Li, *Bioresour. Technol.*, 2013, **133**, 469–474.
7 J. N. Chheda, G. W. Huber and J. A. Dumesic, *Angew. Chem., Int. Ed.*, 2007, **46**, 7164–7183.
8 D. R. Dodds and R. A. Gross, *Science*, 2007, **318**, 1250–1251.
9 C. Gutsche, D. Redmore, R. Buriks, K. Nowotny, H. Grassner and C. Armbruster, *J. Am. Chem. Soc.*, 1967, **89**, 1235.
10 Y. Shigemasa, K. Yokoyama, H. Sashiwa and H. Saimoto, *Tetrahedron Lett.*, 1994, **35**, 1263.
11 G.-W. Wang, Z. Zhang and Y.-W. Dong, *Org. Process Res. Dev.*, 2004, **8**, 18.
12 Z. Zhang, Y.-W. Dong and G.-W. Wang, *Chem. Lett.*, 2003, **32**, 966.
13 V. K. Díez, C. R. Apesteguía and J. I. Di Cosimo, *J. Catal.*, 2006, **240**, 235.
14 C. Noda, G. P. Alt, R. M. Werneck, C. A. Henriques and J. L. F. Monteiro, *Braz. J. Chem. Eng.*, 1998, **15**, 120.
15 I. Di Cosimo, V. K. Diez and C. R. Apesteguia, *Appl. Catal., A*, 1996, **137**, 149.
16 M. J. Climent, A. Corma, S. Iborra and J. Primo, *J. Catal.*, 1995, **151**, 60.
17 B. M. Choudary, M. L. Kantam, P. Sreekanth, T. Bandopadhyay, F. Figueras and A. Tuel, *J. Mol. Catal. A: Chem.*, 1999, **142**, 361.
18 J. Yu, S. Y. Shiau and A. Ko, *Catal. Lett.*, 2001, **77**, 165.
19 M. J. Climent, A. Corma, H. García, R. Guil-López, S. Iborra and V. Fornés, *J. Catal.*, 2001, **193**, 385.
20 H. Naka, Y. Kaneda and T. Kurata, *J. Oleo Sci.*, 2001, **50**, 813.
21 V. Subramoni, V. K. Rajeevan and B. R. Prasad, *Ion Exch. Technol.*, 1984, 367.
22 J. C. A. A. Roelofs, A. J. van Dillen and K. P. de Jong, *Catal. Today*, 2000, **60**, 297.
23 M. J. Climent, A. Corma, S. Iborra and A. Velty, *Catal. Lett.*, 2002, **79**, 157.
24 C. Noda Pérez, C. A. Pérez, C. A. Henriques and J. L. F. Monteiro, *Appl. Catal., A*, 2004, **272**, 229.
25 S. Abelló, F. Medina, D. Tichit, J. Pérez-Ramírez, J. C. Groen, J. E. Sueiras, P. Salagre and Y. Cesteros, *Chem. – Eur. J.*, 2005, **11**, 728.
26 F. Winter, X. Xia, B. P. C. Hereijgers, J. H. Bitter, A. J. van Dillen, M. Muhler and K. P. de Jong, *J. Phys. Chem. B*, 2006, **110**, 9211.
27 R. M. West, Z. Y. Liu, M. Peter, C. A. Gärtner and J. A. Dumesic, *J. Mol. Catal. A: Chem.*, 2008, **296**, 18–27.
28 T. N. Pham, D. Shi and D. E. Resasco, *Appl. Catal., B*, 2014, **145**, 10–23.
29 C. J. Barrett, J. N. Chheda, G. W. Huber and J. A. Dumesic, *Appl. Catal., B*, 2006, **66**, 111–118.
30 R. M. West, Z. Y. Liu, M. Peter, C. A. Gärtner and J. A. Dumesic, *J. Mol. Catal. A: Chem.*, 2008, **296**, 18–27.
31 R. Xing, A. V. Subrahmayam, H. Olcay, W. Qi, P. van Walsum, G. Pendse and G. W. Huber, *Green Chem.*, 2010, **12**, 1933–1946.
32 A. S. Ndou, N. Plint and N. J. Coville, *Appl. Catal., A*, 2003, **251**, 337–345.
33 L. Hora, V. Kelbichová, O. Kikhtyanin, O. Bortnovskiy and D. Kubička, *Catal. Today*, 2014, **223**, 154–162.
34 D. Tichit, M. N. Bennani, F. Figueras, R. Tessier and J. Kervennal, *Appl. Clay Sci.*, 1998, **13**, 401–415.
35 B. F. Sels, D. E. de Vos and P. A. Jacobs, *Catal. Rev. Sci. Eng.*, 2001, **43**, 443–488.
36 W. Shen, G. A. Tompsett, K. D. Hammond, R. Xing, F. Dogan, C. P. Grey, W. C. Conner Jr., S. M. Auerbach and G. W. Huber, *Appl. Catal., A*, 2011, **392**, 57–68.
37 P. A. Zapata, J. Faria, M. P. Ruiz and D. E. Resasco, *Top. Catal.*, 2012, **55**, 38–52.
38 A. Dhakshinamoorthy, M. Opanasenko, J. Čejka and H. Garcia, *Adv. Synth. Catal.*, 2013, **355**, 247–268.
39 A. Dhakshinamoorthy, M. Opanasenko, J. Čejka and H. Garcia, *Catal. Sci. Technol.*, 2013, **3**, 5209–5240.
40 D. P. Debecker, E. M. Gaigneaux and G. Busta, *Chem. – Eur. J.*, 2009, **15**, 3920–3393.
41 C. Xu, Y. Gao, X. Liu, R. Xin and Z. Wang, *RSC Adv.*, 2013, **3**, 793–801.
42 S. Abelló, D. Vijaya-Shankar and J. Pérez-Ramírez, *Appl. Catal., A*, 2008, **342**, 119–125.
43 E. Taarning, C. Osmundsen, X. Yang, B. Voss, S. Andersen and C. Christensen, *Energy Environ. Sci.*, 2011, **4**(3), 793–804.
44 C. Perego and D. Bianchi, *Chem. Eng. J.*, 2010, **161**(3), 314–322.
45 H. van Bekkum and H. W. Kouwenhoven, *Stud. Surf. Sci. Catal.*, 2007, **168**, 947–998.
46 A. Corma, S. Iborra and A. Velty, *Chem. Rev.*, 2007, **107**(6), 2411–2502.
47 P. Mäki-Arvela, B. Holmbom, T. Salmi and D. Murzin, *Catal. Rev. Sci. Eng.*, 2007, **49**(3), 197–340.
48 M. Bejblová, D. Procházková and J. Čejka, *ChemSusChem*, 2009, **2**, 486.
49 E. Dumitriu, V. Hulea, I. Fechete, A. Auroux, J.-F. Lacaze and C. Guimon, *Microporous Mesoporous Mater.*, 2001, **43**, 341–359.
50 A. Ungureanu, S. Royer, T. V. Hoang, D. Trong On, E. Dumitriu and S. Kaliaguine, *Microporous Mesoporous Mater.*, 2005, **84**, 283–296.
51 T. Komatsu, M. Mitsuhashi and T. Yashima, *Stud. Surf. Sci. Catal.*, 2002, **142**, 667–674.

52 O. Kikhtyanin, V. Kelbichová, D. Vitvarová, M. Kubů and D. Kubička, *Catal. Today*, 2014, **227**, 154–162.
53 W. J. Roth, C. T. Kresge, J. C. Vartuli, M. E. Leonowicz, A. S. Fung and S. B. McCullen, *Stud. Surf. Sci. Catal.*, 1995, **94**, 301.
54 F. S. O. Ramos, M. K. De Pietre and H. O. Pastore, *RSC Adv.*, 2013, **3**, 2084.
55 W. J. Roth, P. Nachtigall, R. E. Morris, P. S. Wheatley, V. R. Seymour, S. E. Ashbrook, P. Chlubná, L. Grajciar, M. Položij, A. Zukal, O. Shvets and J. Čejka, *Nat. Chem.*, 2013, **5**, 628.
56 W. J. Roth, P. Nachtigall, R. E. Morris and J. Čejka, *Chem. Rev.*, 2014, DOI: 10.1021/cr400600f, article ASAP.
57 W. J. Roth, in *Introduction to Zeolite Science and Practice*, ed. J. Čejka, H. V. Bekkum, A. Corma, F. Schuth, Elsevier Science, 2007, vol. 168.
58 M. E. Leonowicz, S. L. Lawton, R. D. Partridge, P. Chu and M. K. Rubin, *Science*, 1994, **264**, 1910.
59 S. L. Lawton, M. E. Leonowicz, R. D. Partridge, P. Chu and M. K. Rubin, *Microporous Mesoporous Mater.*, 1998, **23**, 109–117.
60 S. Maheshwari, C. Martínez, M. T. Portilla, F. J. Llopis, A. Corma and M. Tsapatsis, *J. Catal.*, 2010, **272**, 298–308.
61 S. Lawton, A. Fung, G. Kennedy, L. Alemany, C. Chang, G. Hatzikos, D. Lissy, M. Rubin, H. Timken and S. Steuernagel, *J. Phys. Chem.*, 1996, **100**, 3788.
62 K. Liu, S. Xie, S. Liu, G. Xu, N. Gao and L. Xu, *J. Catal.*, 2011, **283**, 68–74.
63 G. G. Juttu and R. F. Lobo, *Microporous Mesoporous Mater.*, 2000, **40**, 9–23.
64 Y. J. He, G. S. Nivarthy, F. Eder, K. Seshan and J. A. Lercher, *Microporous Mesoporous Mater.*, 1998, **25**, 207–224.
65 Y. Zhang, H. Xing, P. Yang, P. Wu, M. Jia, J. Sun and T. Wu, *React. Kinet. Catal. Lett.*, 2007, **90**, 45–52.
66 S. Brunauer, P. H. Emmet and E. Teller, *J. Am. Chem. Soc.*, 1938, **62**, 309.
67 B. C. Lippens and J. H. de Boer, *J. Catal.*, 1965, **4**, 319.
68 B. Gil, S. I. Zones, S.-J. Hwang, M. Bejblová and J. Čejka, *J. Phys. Chem. C*, 2008, **112**, 2997.
69 A. Corma, V. Fornés, L. Forni, F. Márquez, J. M. Triguero and D. Moscotti, *J. Catal.*, 1998, **179**, 451–458.
70 P. Chlubná, W. J. Roth, A. Zukal, M. Kubů and J. Pavlatová, *Catal. Today*, 2012, **179**, 35–42.
71 K. S. W. Sing, D. H. Everett, F. A. W. Haul, L. Mouscou, R. A. Pierotti, J. Rouquerol and T. Siemieniewska, *Pure Appl. Chem.*, 1985, **57**, 603.
72 M. Kruk, M. Jaroniec and A. Sayari, *J. Phys. Chem. B*, 1997, **101**, 583.
73 F. Rouquerol, J. Rouquerol and K. Sing, *Adsorption by Powders and Porous Solids, Principles Methodology and Applications*, Academic Press, London, 1999.
74 J. S. Beck, J. C. Vartuli, W. J. Roth, M. E. Leonowicz, C. T. Kresge, K. D. Schmitt, C. T.-W. Chu, D. H. Olson, E. W. Sheppard, S. B. McCullen, J. B. Higgins and J. L. Schlenker, *J. Am. Chem. Soc.*, 1992, **114**, 10834.
75 O. Franke, J. Rathousky, G. Schulz-Ekloff, J. Stárek and A. Zukal, in *Zeolites and Related Microporous Materials: State of the Art 1994, Studies in Surface Science and Catalysis*, ed. J. Weitkamp, H. G. Karge, H. Pfeifer and W. Hölderich, vol. 84, Part B, Elsevier, Amsterdam, 1994, p. 77.
76 A. Corma, U. Diaz, V. Fornés, J. M. Guil, J. Martínez-Triguero and E. J. Creyghton, *J. Catal.*, 2000, **191**, 218–224.
77 S. Laforge, P. Ayrault, D. Martin and M. Guisnet, *Appl. Catal., A*, 2005, **279**, 79–88.
78 A. Corma, V. Fornes, J. Martinez-Triguero and S. B. Pergher, *J. Catal.*, 1999, **186**, 57–63.
79 A. Lercher, C. Grundling and G. Eder-Mirth, *Catal. Today*, 1996, **27**, 353.
80 B. Gil, B. Marszałek, A. Micek-Ilnicka and Z. Olejniczak, *Top. Catal.*, 2010, **53**, 1340.
81 E. J. A. Schweitzer and P. F. Van den Oosterkamp, *Microporous Mesoporous Mater.*, 1998, **20**, 397.